Texas A&M University
Mechanical Engineering Department
Turbomachinery Laboratory
Tribology Group

Identification of Structural Stiffness and Material Loss Factor in a Shimmed (Generation One) Bump Type Foil Bearing

Research Progress Report to the TAMU Turbomachinery Research Consortium

TRC-B&C-04-13

By

Luis San Andrés
Mast-Childs Tribology Professor
Principal Investigator

Joshua David Norsworthy
Research Assistant

May 2013

Shimmed Bump-Type Foil Bearings For Oil-Free Turbomachinery

TRC Project, TEES # 32513/1519 FB

Executive Summary

Bump-type foil bearings (BFB) provide reliable support with low drag power losses to oil-free micro turbomachinery (<400 kW). Despite the advantages that BFBs offer, rotors supported on BFBs often display large amplitude subsynchronous whirl motions. The performance and stability of BFB supported rotors dependents on the BFB underspring support structure, i.e., the top foil and bump foil strips. Prior research identifies shimming as a low cost method of increasing the stiffness and damping of BFBs leading to improved rotordyanmic performance of BFB supported rotors.

This report characterizes the structural stiffness (K) and material loss factor (γ) of a first generation BFB with shims. A 26 bump test bearing with nominal radial clearance of 0.12 mm (L=38.1 mm, D=36.5 mm) is tested under static loads. Three steel shims of 50 μm and 100 μm thickness are affixed to the inner surface of the bearing cartridge to add a mechanical preload. A simple (non rotating shaft) test rig is assembled on a lathe to measure the FB deflection due to applied static loads (F). Tests are conducted for two bearing orientations (defined by the position of the top foil fixed end relative to the direction of applied load) and for three configurations (shimless, with 50 μm shims, and with 100 μm shims). Test results show a nonlinear bearing deflection versus load behavior. Increasing the mechanical preload (adding shims) effectively reduces the bearing clearance. Multiple loading and unloading cycles evidence little mechanical energy dissipation for all bearing configurations.

The BFB structural stiffness increases with increasing shim thickness as well as increasing loads. For a 100 N load (F/LD=0.75 bar) the BFB structural stiffness for the 50 μm shim BFB configuration is 17% higher than the bearing without shims and the structural stiffness for the bearing with 100 μm shims is 45% higher than that of the bearing without shims. Predictions of load versus BFB deflection and structural stiffness from a simple computational tool compare well against the experimental results.

The mechanical energy dissipation capability of a BFB is best described by a material loss factor. The original bearing (without shims) has a small loss factor γ~0.02. The bump foil bearing with 100 μm shims shows a loss factor (γ~0.07) slightly higher than the original bearing but lower than the bearing with 50 μm shims (γ~0.20).

Table of Contents

Identification of Structural Stiffness and Material Loss Factor in a Shimmed (Generation One) Bump-Type Foil Bearing

Luis San Andrés and Joshua Norsworthy, May 2013

List of Tables

List of Figures

Nomenclature

c_{nom}	Nominal radial clearance[mm]
$c_{(\theta)}$	Radial clearance [mm]
D_I	Bearing cartridge inner diameter [mm]
D_O	Bearing cartridge outer diameter [mm]
D_s	Shaft diameter [mm]
E	Elastic modulus of the top foil and bump foil materials [Pa]
E_{dis}	Dissipated mechanical energy [Nm]
$F_{(x)}$	BFB structural reaction force [N]
F	Applied static load [N]
F_s	$K_e\delta$, Maximum static load [N]
h_B	Bump height [mm]
$I_{(\alpha)}$	Geometric function of bump arc (α)
$J_{(\alpha)}$	Geometric function of bump arc (α)
$K_{(z_1)}$	Bearing structural stiffness [MN/m]
$K_{0\text{-}3}$	Polynomial curve fit coefficients of load versus BFB deflection results
K_s	Shaft stiffness [MN/m]
K_e	Effective BFB structural stiffness of ($=F_s/\delta$) [MN/m]
κ_w	Stiffness per unit area of a bump with both ends fixed [MN/m^3]
κ_f	Stiffness per unit area of a bump with one end fixed and one end free [MN/m^3]
L	Bearing axial length [mm]
l_B	Bump length [mm]
l_0	Bump half length [mm]
N_B	Number of Bumps
N_S	Number of shims
p	Bump pitch [mm]
s_0	Bump pitch [mm]
t_B	Bump foil thickness [mm]
t_S	shim thickness [mm]
t_T	Top foil thickness [mm]

W	Bearing weight [10 N]
x	Foil bearing displacement [mm]
x_a, x_b	Location of initial bump deflection from positive and negative loads, respectively [mm]
α	Bump height angle [°]
γ	Material loss factor
δ	Maximum bump deflection under static load F_s [mm]
θ	Bearing angular location [°]
θ_1	Angular location of the first shim (counter-clockwise rotation) [°]
θ_p	Angular distance between shims [120°]
μ_f	Dry friction coefficient between the bearing cartridge inner surface and the bump foil strip
v	Poisson's ratio of the top foil and bump foil material

Introduction

Oil free microturbomachinery (<400 kW) implements gas foil bearing (GFB) technology, in particular bump type foil bearings, to provide reliable supports with low drag at high speed operation [1]. Bump type foil bearings (BFB) typically comprise of one or more bump foil strip layers, a top foil, and a bearing cartridge. At a sufficiently high rotor speed hydrodynamic pressure develops, forcing a gap between the rotor and the top foil, thus lifting the rotor and avoiding contact with the bearing housing. During airborne operation, the hydrodynamic gas pressure in series with the elastic bump foil structure support external loads. Mechanical energy dissipation is important for the stability of the rotor bearing system and is provided by the bumps underspring structure. Energy is dissipated in the form of Coulomb dry friction arising from the relative motion of the bump foil strips pressed against the bearing cartridge and the bump foil crests with the top foil. To a minor extent viscous drag from the air film also adds damping to the bearing.

Brief Review of Relevant Literature

BFBs are capable of satisfying the requirements of high-speed micro-turbomachinary (<400 kW) [2]. However rotors supported on BFBs often show large subharmonic whirl motions usually mistaken as a rotordynamic instability [3]. The subharmonic whirl motions may track the shaft speed or become locked at a rotor natural frequency [4]. Excessive amplitudes of rotor vibration can result in failure of the rotor-bearing systems (RBS) [4]. This section reviews some of the literature reporting subsynchronous whirl motions in BFB supported rotors and the known procedures to ameliorate this undesirable behavior.

Kim and San Andrés [5] observe large amplitude (56 μm) subharmonic motions in speed coast down measurements of a rotor supported on BFBs. The whirl motions have a frequency equal to 1/2 and 1/3 of the synchronous speed. Subsynchronous vibrations are ascribed to the nonlinear stiffness characteristics of the FB structure and are exacerbated by the presence of rotor imbalance. Kim and San Andrés note that the performance of RBS is largely dependent on the underspring structural characteristics and that foil bearings implementation into a RBS requires careful design with the entire system in consideration. Ref. [5] reviews the prior literature giving many more examples of RBSs displaying subsynchronous motion responses.

Rubio and San Andrés [4] demonstrate that an increase in air feed pressurization reduces the amplitude of subsynchronous whirl motions in a rotor supported on BFBs and while it crosses system natural frequencies. External pressurization has no effect on the rotor synchronous motion amplitude response for operation well above critical speeds. A model of GFBs with side pressurization advanced in Ref. [4] predicts increased direct stiffness and damping coefficients as well as reduced cross-coupled stiffness coefficients as the feed pressure rises. Decreased cross-coupled stiffnesses increase the stability of rotor-bearing systems (RBS). Ref.[4] thus reports a method to reduce subsynchronous whirl motion amplitudes, thereby improving the stability of a RBS.

Kim and San Andrés [2] investigate the dynamic response of a rotor supported on mechanically preloaded (shimmed) bearings. The preload, introduced by affixing metal shims to the inner surface of the bearing cartridge, effectively introduces a hydrodynamic wedge that increases the hydrodynamic film pressure, leading to an increase in load capacity. Rotor coast down responses are obtained for a rotor supported on both BFBs with and without shims. The response of a rotor supported on bearing without shims shows large amplitudes subsynchronous whirl motion (50 μm) for rotor speeds ranging from 27 krpm and 50 krpm with low feed pressure (0.35 bar). Under the same test conditions, the rotor supported on shimmed bearings shows smaller subsynchronous whirl amplitudes (20 μm) over a smaller shaft speed range (38 krpm to 50 krpm). The tests results in Ref. [2] demonstrate that mechanical preload reduces the severity of rotor subsynchronous whirl motions as well as delays their onset. This information has the potential to extend the life of high-speed rotating machinery.

BFBs can improve the performance of automobile turbochargers (TC) by reducing drag power losses thereby increasing their efficiency. Ref. [3] presents measurements of static load-deflection tests for test BFBs with and without shims, measurements of performance in a compressed air driven oil free TC supported on the test BFBs, as well as preliminary measurements of an oil-free TC driven by a vehicle diesel engine. Three metal shims (thickness 0.03 mm) are affixed to one BFB as in Ref. [2]. Test results from multiple cycles of push and pull loads effectively identify the bearing clearances, and also evidence structural damping in both BFBs. The structural stiffness coefficients are determined from the load-deflection data in both test BFBs. Results show that adding shims increases the bearing direct stiffness coefficients, thus displacing critical speeds to higher magnitudes.

In Ref. [3] a pressurized air driven TC is revamped to incorporate one test BFB and a thrust foil bearing. Rotor speed coast down experiments (from 82 krpm) were conducted for bearings with and without shims. Rotor response data from waterfall plots demonstrate that a shimmed foil bearing delays the onset speed of subsynchronous whirl motions and attenuates their amplitude in the TC. The test setup is modified to allow the TC to be driven by a diesel engine. Results consistently reveal an improved rotordynamic performance for rotors supported on shimmed bearings. The authors note that TC rotor speed versus diesel engine speed data evidences that shimmed BFBs may have slightly higher drag power losses. No results of drag torque or power loss are presented in Ref. [3].

Schiffmann and Spakovsky [6] investigate (numerically) the role of underspring stiffness, structural damping, and static load on the rotordynamic stability of a rigid rotor supported on first generation BFBs. Ref. [6] reports that decreasing the bearing underspring compliance (increasing its stiffness) and increasing the static load can significantly improve the RBS stability (critical mass) and increase the onset speed of instability while structural damping has only a marginal effect. The authors note that an increased static load affects the fluid film thickness and the pressure distribution such that the ratio of cross-coupled and direct force coefficients (stiffness and damping) decreases thereby improving stability. The authors conjecture that tailoring the fluid film pressure profile by introducing shims at specific circumferential locations (selective shimming) is a means to increase the system onset speed of instability. Furthermore, Schiffman and Spakovsky produce design guidelines and optimum shim patterns for improved FB stability. While these optimum shim patterns promise improved rotordynamic stability for BFB supported rotors, a single shim pattern requires shims of thickness ranging from 50% to 90% of the bearing clearance. The availability of shims of very particular thickness is limited, making the shim patterns impractical.

The objective of the current work is to experimentally measure and to compare the structural characteristics of a BFB with and without shims by estimating the structural stiffness and material loss factor from applied static loads. In the limited tests reported, the shaft does not rotate.

Test Foil Bearing

A series of static and dynamic load tests were carried out on a first generation BFB. A mechanical preload is added to the BFB structure by inserting shims of known thickness. Figure 1 presents a schematic view of a typical BFB with shims added at discrete circumferential locations. The inset shows an enlarged view of the region surrounding an individual shim.

Table 1 shows the dimensions of the test bearing, test shaft, and metal shims and Figure 2 depicts a photograph of a bump foil bearing with a metal shim inserted between the bearing cartridge and the bump foil layers. Each bump is a simple elastic element. Note that the individual bumps sitting atop shims (hereby referred to as shimmed bumps) are pressed closer to the rotor than other bumps. As a result, during loading, the shimmed bumps are engaged before other bumps.

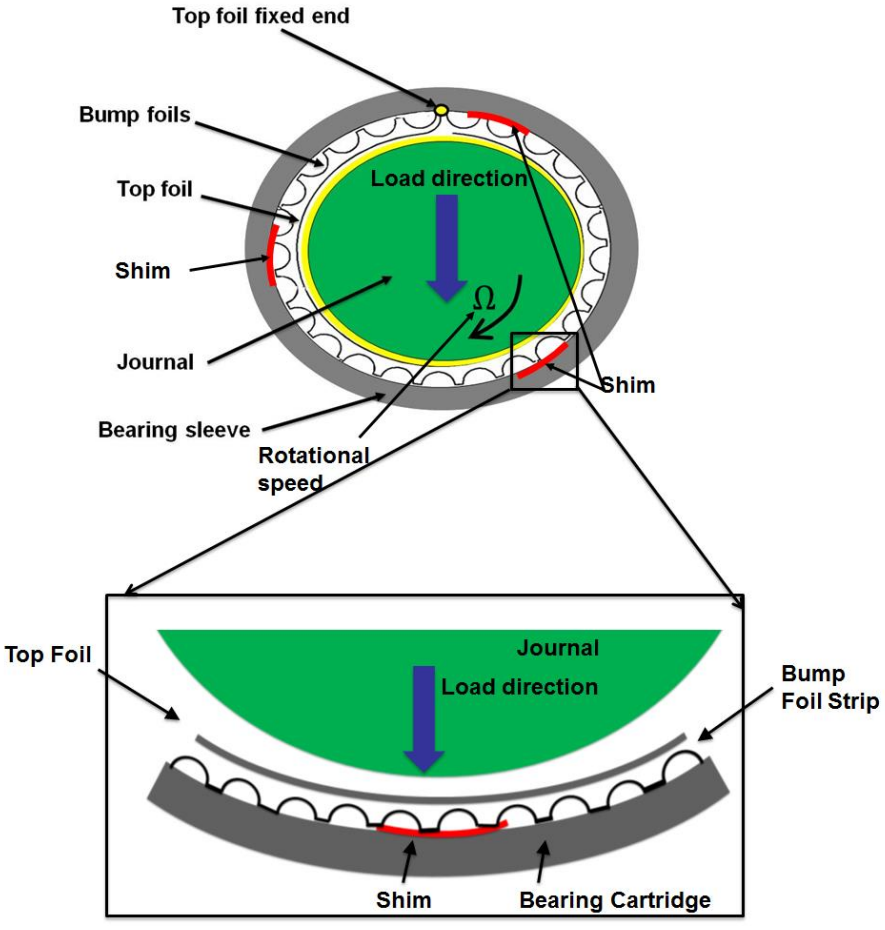

Fig. 1 Schematic representation of a first generation bump-type foil bearing with metal shims. Inset shows a zoomed in view of the area around a shim.

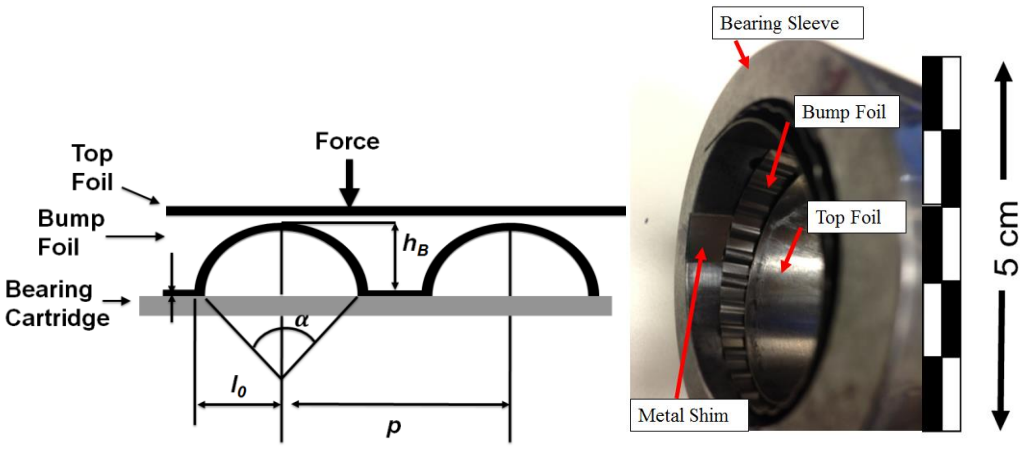

(a) **(b)**

Fig. 2 (a) Schematic of bump foil with dimensional parameters [7], and (b) a photograph of a BFB with a metal shim layered axially through the bearing.

Table 1 Nominal dimensions of the test foil bearing and metal shims.

Parameters	**Magnitude**
Bearing cartridge outer diameter, D_O	50.74 mm
Bearing cartridge inner diameter, D_I	37.98 mm
Bearing axial length, L	38.10 mm
Top foil thickness (Inconel X750), t_T	0.1 mm
Foil length , $2\pi D_I$	110 mm
Elastic modulus, E	214 GPa
Poisson's ratio, ν	0.29
Number of bumps, N_B	26
Bump foil (Inconel X750)	
Thickness, t_B	0.112 mm
Pitch, s_0	4.5 mm
Length, l_B	2.5 mm
Height, h	0.50 mm
Elastic modulus, E	214 GPa
Poisson's ratio, ν	0.29
Shim (AISI 4140)	
Length	38.1 mm
Thickness, t_s	0.050 mm
Width	7.87 mm
Angular extent	11.8°
Elastic modulus, E	214 GPa
Poisson's ratio, ν	0.29
Shaft diameter, D_s	36.5 mm
Measured inner diameter of the FB (assembled)	36.74 mm
Nominal FB radial clearance, $c_{nom} = (D_I - D_s)/2$	0.120 mm
Weight of test bearing and outer cartridge, W	10 N

The shaft is made of AISI 4140 steel and the BFB, manufactured by the Korean Institute of Science and Technology (KIST), consists of a top foil and a single underspring layer with 26 bumps. Both foils are uncoated and made of Inconel X750. The bearing fits inside an outer cartridge that allows the attachement of sensors.

The addition of metal shims changes the bearing clearance profile. Figure 3 shows the bearing radial clearance relative to the nominal radial clearance (c_{nom}=120 μm) versus angular location for increasing shim thickness. The clearance profile in a bearing with three equally spaced shims of known thickness, t_s, and nominal clearance, c_{nom}, is [2]

$$c_{(\theta)} = \left(1 - \frac{t_s}{2c_{nom}}\right) c_{nom} - \frac{1}{2} t_s \cos\left[\left(N_s(\theta - \theta_1 - \theta_p)\right)\right]$$

where θ is an arbitrary angular location, θ_1 is the angular location of the middle of a first shim (counter clockwise direction), and θ_p (=120°) is the angular space between shims. Note that the clearance of a bearing with shims is periodic and resembles that in a tri-lobe bearing. For a bearing with both 50 μm shims and 100 μm shims, the clearance at the location of the shims reduces by 40% and 80%, respectively. The addition of increasingly thicker shims leads to a condition of interference fit.

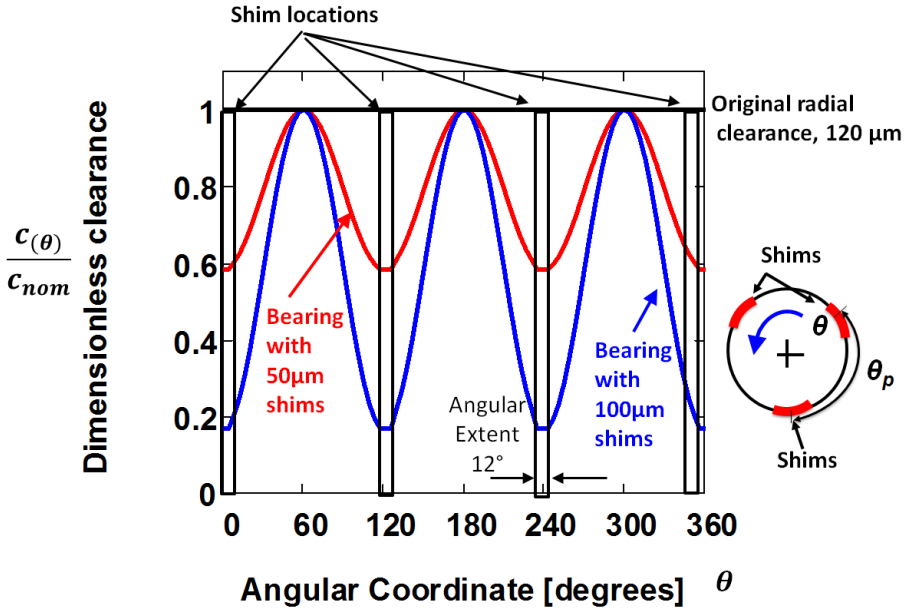

Fig. 3 Dimensionless clearance profile of a bump foil bearing versus angular coordinates (θ) for two shim thicknesses (50 μm and 100 μm). Nominal radial clearance is 120 μm.

Test Rig Description

The tests setup to apply push and pull loads is shown in Figure 4 and consists of a lathe chuck and tool holder, an eddy current sensor, a load cell, and a nonrotating shaft. The lathe provides a solid stationary foundation, and the forward and backward motion of the tool holder makes the loading mechanism. Figure 5 presents a schematic view of the shimmed BFB, showing the procedure for applying static loads to the bearing. Static load test are conducted on the bearing without shims and with shims of thickness 50 μm and 100 μm. One shim is installed 45° from the fixed end of the top foil and act as a reference for the position of the other shims. Each shim has an adhesive coating on one side (unknown thickness) that affixes it to the inner diameter of the bearing housing. Note that the 100 μm shim thickness is introduced by stacking two metal shims of 50 μm thickness.

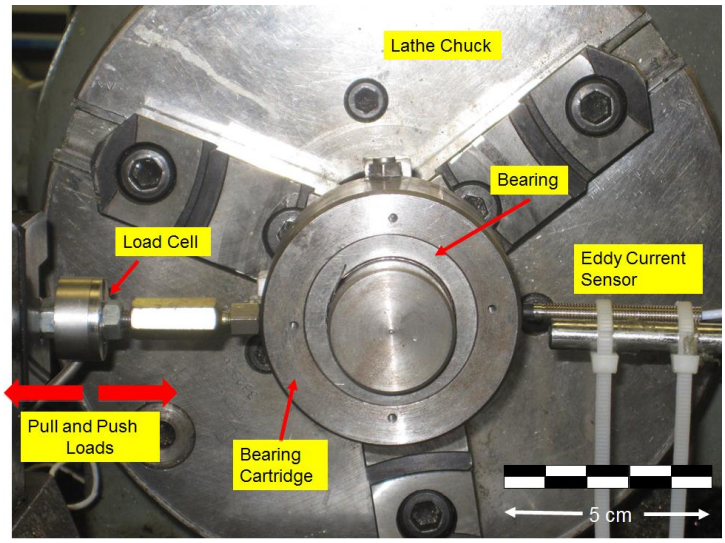

Fig. 4 Test setup for static push and pull load tests on a BFB.

One end of the shaft is affixed in a lathe chuck. An eddy current sensor measures the horizontal displacement of the bearing, and a strain gauge type load cell measures the static load. One end of the load cell is threaded directly to the bearing outer cartridge mid-span via a stinger rod, and the other is affixed to the lathe tool holder.

Note in Figure 5 that the top foil fixed end is installed at either 45° or 90°away from the direction of the load applied along the horizontal direction. Also the bearing weight (W=10 N

W/LD=7.5 kPa or 1.09 psi) acts vertically, i.e., 90° away from the direction of the applied static load.

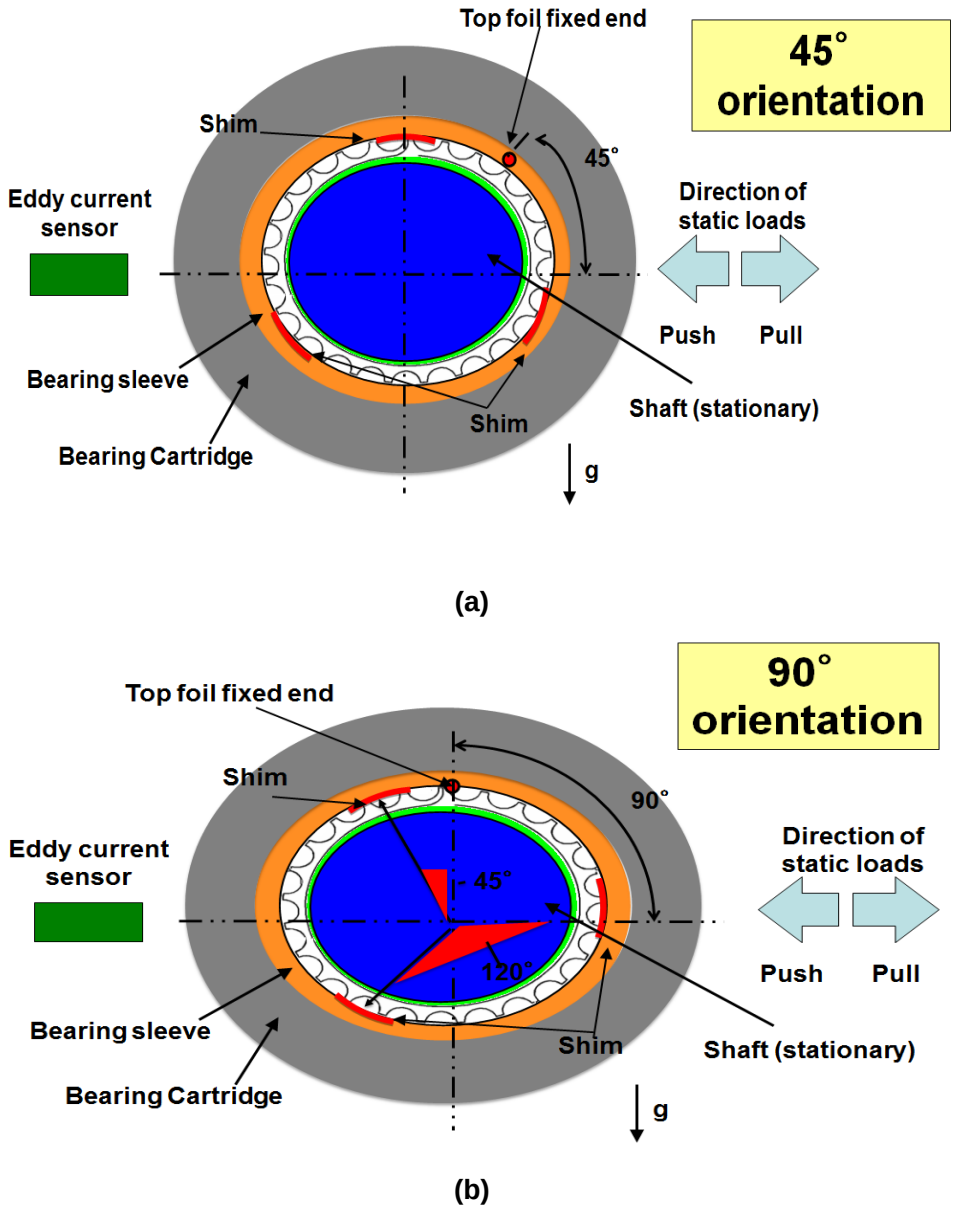

Fig. 5 Schematic views of shimmed BFBs under static push and pull loads (a) 45° and (b) 90° bearing orientations relative to the fixed end of the top foil.

Even though the lathe provides a stationary platform for the measurements, the test shaft deflects under the application of push and pull loads. The stiffness of the shaft alone (K_s) is 7.11 MN/m as identified from earlier load versus deflection results. The deflection of the test bearing alone is then determined by subtracting the displacement of the shaft from the measured absolute displacement of the test system (bearing and shaft). Push loads (up to 200 N) are applied first to

the test shaft and the deflection of the shaft is recorded. The maximum deflection experienced by the shaft over the applied load range is 27 μm. The static load versus shaft deflection behavior is linear up to 200 N.

Results of Static Force versus Deflection and Identification of Bump Foil Bearing Structural Stiffness

Figure 6 shows the measured FB displacement (x) for the original bearing (without shims) for four cycles of load and unload force (F). The data for all tests is shifted about the zero deflection condition to simulate symmetry. Table 2 lists the extent and direction denoted by the plus or minus of the data shift. As the shim thickness increases, the extent of the shift decreases. Note also that for most tests, the data was shifted towards the negative side of the zero deflection condition, i.e., $x<0$. This result demonstrates that the bearing was not centered on the shaft. The off-centered position of the bearing is partially due to the bearing resting atop the shaft during loading, and to the process of installing the bearing and loading apparatus. The values of the displacement data shift vary for all test conditions, indicating that the operator inconsistently assembled the bearing on the test shaft.

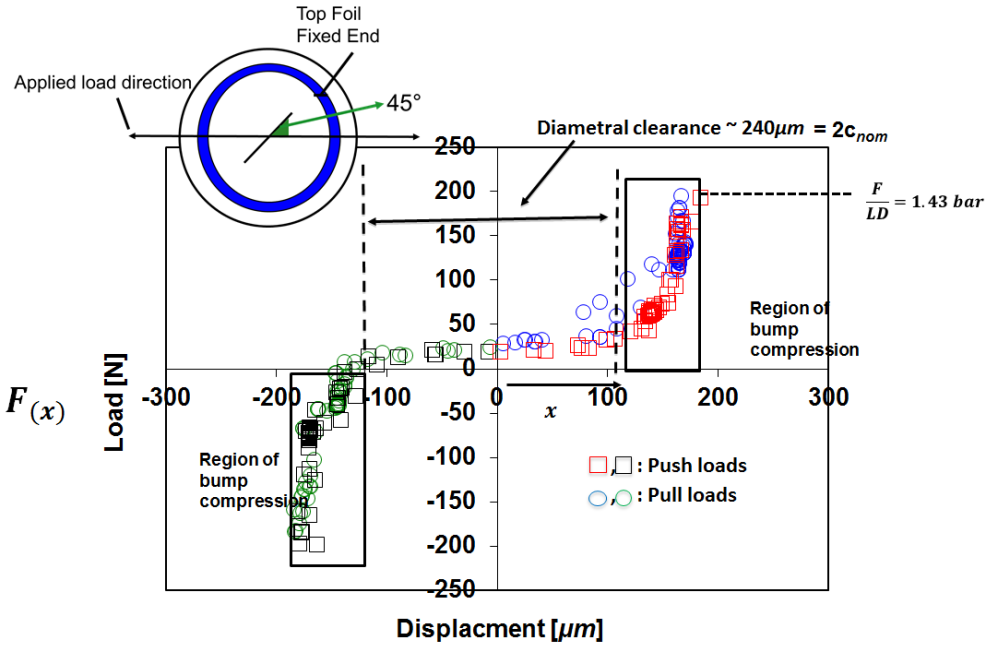

Fig. 6 Static push and pull loads versus deflection for a BFB without shims, 45° bearing orientation.

Table 2 Extent and direction of displacement data shift for all tests conditions.

Bearing Configuration		Shift [μm]
45°	Original	-110
	50μm shims	-40
	100μm shims	-10
90°	Original	-60
	50μm shims	-20
	100μm shims	+20

Results from all tests show a similar nonlinear behavior. Load versus bearing deflection results for all configurations show miniscule mechanical hysteresis loops, evidencing small amounts of mechanical energy dissipation due to dry friction. Load versus FB deflection results for the original bearing and a BFB with 50 μm shims show a "deadband" i.e., a section where the bearing experiences large displacements with small changes in force. This "deadband" section evidences the clearance of the bearing, i.e., a gap between the top foil inner diameter and the shaft outer diameter. Table 3 presents the initial locations of bump compression (x_a , and x_b) that bound the clearance region. Note that $|x_b| \sim x_a$ due to the shift imposed on the load versus bearing deflection results.

Table 3 Location of initial bump deflection for all tests conditions.

Bearing Configuration		x_a [μm]	x_b [μm]
45°	Original	100	-100
	50 μm shims	55	-55
	100 μm shims	0	0
90°	Original	100	-100
	50 μm shims	55	-55
	100 μm shims	0	0

The bearing rests atop the rotor during static load tests and thus the top foil is in contact with the rotor. Prior to bump compression the top foil surface moves relative to the rotor creating a small friction force that the applied load must overcome to move the bearing. This behavior gives rise to an applied load greater than zero when there is no bump deflection as seen in the experimental results. Note that the uncertainty in the load measurements is ± 4.4 N

The data reduction procedure separates the load versus deflection curves into two distinct regions; one for positive loads and one for negative loads. The two regions of the load versus FB deflection data are fitted to a cubic polynomial.

For $x > x_a$, on the right side of the load versus bearing deflection data curve (see Figure 6),

$$F_{(x)} = K_{a0} + K_{a1}x + K_{a3}x^3 \quad (1)$$

where $\{K_{a\beta}\}_{\beta=1,2,3}$ are polynomial fit coefficients for $x > x_a$

For $x < x_b$

$$F_{(z_2)} = K_{b0} + K_{b1}x + K_{b3}x^3 \quad (2)$$

where $\{K_{b\beta}\}_{\beta=1,2,3}$ are the polynomial fit coefficients for $x < x_b$. No analysis is conducted for the region $x_b \leq x \leq x_a$, i.e., the deadband region. Table 4 and 5 presents the curve fit coefficients for each tests condition under push and pull loads for the region of positive and negative loads as well as the correlation coefficient, indicating the goodness of the fit.

Table 6 presents the bearing radial clearances as estimated from the load versus bearing deflection data for each bearing configuration. The reductions in clearance correspond well with the shim thickness for the bearing configurations with 50 μm shims. The uncertainty in the radial clearance estimations is ±0.70 μm.

The bearing with the 100 μm shims installed is expected to show a 20 μm radial clearance (as shown in Figure 3). However, the load versus bearing deflection results for the bearing with 100 μm shims do not show a deadband suggesting that there is an assembly interference preload, i.e., the inner diameter of the bearing is smaller than the outer diameter of the rotor. The adhesive used to affix the shims to the bearing cartridge is the source of added thickness. The thickness of one shim and glue layer is 100 μm, which is much larger than the manufacturer specified metal thickness (50 μm). This increase in thickness is due to the glue on the underside of the shim. While the glue layer adds to the shim thickness, it is compressible and thus the actual thickness of the glue layer during loading is unknown. Tests conducted on a bearing with 50 μm shims do not show a decreased clearance due the glue layer however.

Table 4 Coefficients of curve fit polynomials describing force versus deflection for the region of $x \geq x_a$.

Bearing Configuration			$F=K_{a0}+K_{a1}x+K_{a1}x^3$			Range of validity (μm)		
			K_{a0} [N]	K_{a1} [N/μm]	K_{a3} [N/μm^3]	x_a	x_{max}	R^2
45°	Original	Push Loads	37	-0.40	$3.1\text{x}10^{-5}$	100	160	0.98
		Pull Loads	31	-0.10	$2.5\text{x}10^{-5}$	100	160	0.99
	50 μm shims	Push Loads	16	-0.05	$5.2\text{x}10^{-5}$	50	120	0.98
		Pull Loads	13	0.55	$1.3\text{x}10^{-5}$	50	120	0.99
	100 μm shims	Push Loads	-41	1.84	$3.0\text{x}10^{-4}$	0	60	0.98
		Pull Loads	-40	1.79	$3.0\text{x}10^{-4}$	0	60	0.98
90°	Original	Push Loads	16	-0.18	$2.2\text{x}10^{-5}$	100	160	0.99
		Pull loads	26	-0.07	$1.6\text{x}10^{-5}$	100	160	0.98
	50 μm shims	Push Loads	24	-0.08	$5.1\text{x}10^{-5}$	50	120	0.97
		Pull Loads	18	-0.17	$5.6\text{x}10^{-5}$	50	120	0.99
	100 μm shims	Push Loads	24	1.58	$4.0\text{x}10^{-4}$	0	60	0.98
		Pull Loads	-34	1.90	$2.0\text{x}10^{-4}$	0	60	0.98

Table 5 Coefficients of curve fit polynomials describing force versus deflection FB for the region of $x \le x_b$.

Bearing Configuration			$F=K_{b0}+K_{b1}x+K_{b3}x^3$			Range of validity (μm)		
			K_{b0} [N]	K_{b1} [N/μm]	K_{b3} [N/μm^3]	x_b	x_{max}	R^2
45°	Original	Push Loads	5.7	-0.40	$3.1\text{x}10^{-5}$	-100	-160	0.98
		Pull Loads	15	-0.69	$5.0\text{x}10^{-5}$	-100	-160	0.99
	50 μm shims	Push Loads	16	0.12	$3.6\text{x}10^{-5}$	-50	-120	0.98
		Pull Loads	32	0.68	$2.2\text{x}10^{-5}$	-50	-120	0.99
	100 μm shims	Push Loads	-41	1.84	$3.0\text{x}10^{-4}$	0	-60	0.98
		Pull Loads	-40	1.79	$3.0\text{x}10^{-4}$	0	-60	0.98
90°	Original	Push Loads	9.9	-0.04	$2.8\text{x}10^{-5}$	-100	-160	0.99
		Pull loads	7.0	-0.17	$3.7\text{x}10^{-5}$	-100	-160	0.98
	50 μm shims	Push Loads	15	0.35	$3.3\text{x}10^{-5}$	-50	-120	0.97
		Pull Loads	19	0.35	$5.0\text{x}10^{-5}$	-50	-120	0.99
	100 μm shims	Push Loads	24	1.58	$4.0\text{x}10^{-4}$	0	-60	0.98
		Pull Loads	-34	1.90	$2.0\text{x}10^{-4}$	0	-60	0.98

Table 6 BFB radial clearance as estimated from load versus deflection results (Figure 7)

Bearing Configuration		Estimated Radial Clearance [um]
45°	Original	115
	50μm shims	57
	100μm shims	0
90°	Original	112
	50μm shims	55
	100μm shims	0

Comparison of Results for three Bump-Type Foil Bearings

Figure 7 depict the measured load versus FB deflection for four cycles of applied push and pull loads for each of the bearing configurations. As the shim thickness increases the load versus deflection behavior becomes increasingly narrow evidencing a reduction in gap or clearance.

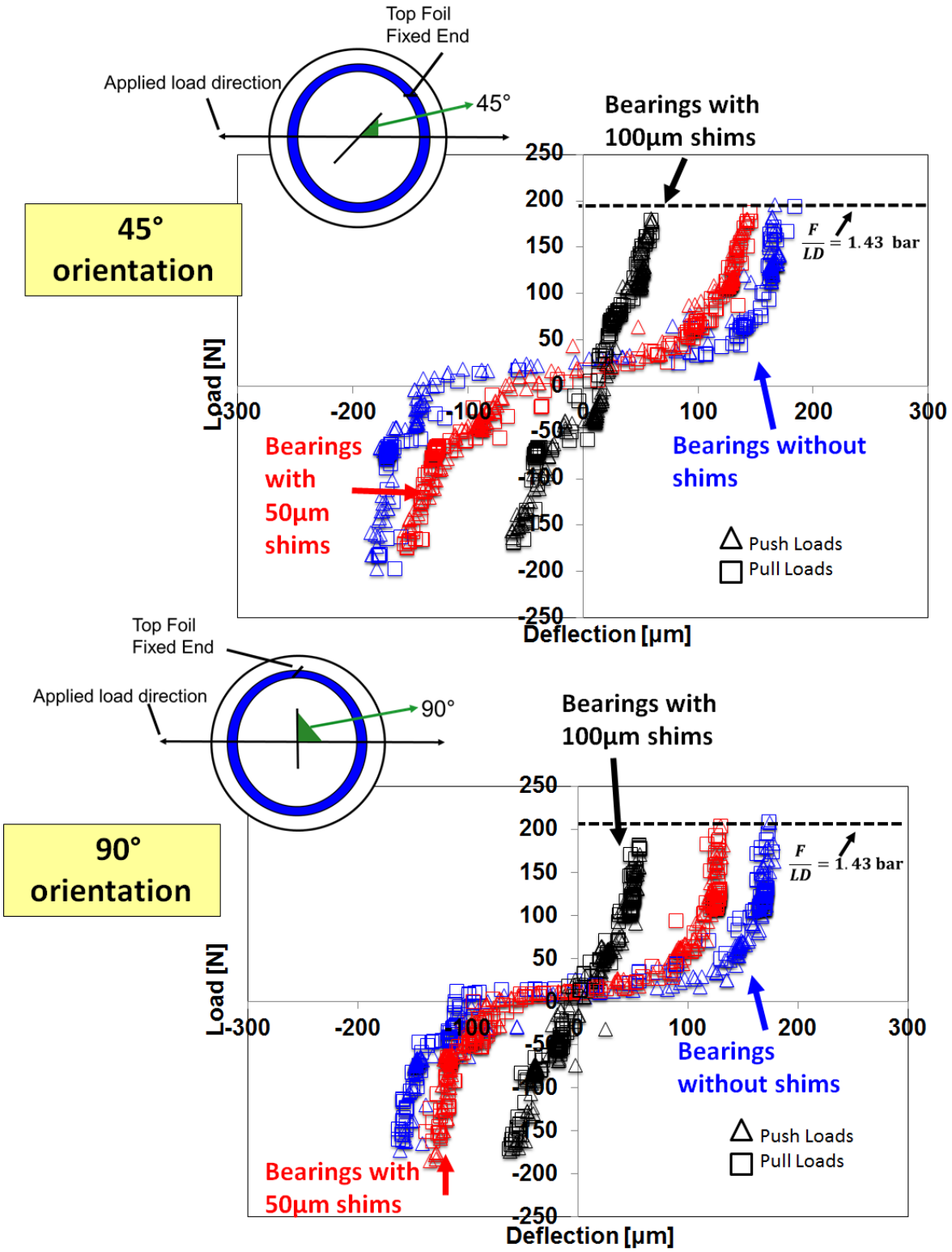

Fig. 7 FB deflection versus static load for the (top) 45° and (bottom) 90° bearing orientation. 4 cycles of push and pull loads are shown for three shim BFB configurations (0 µm, 50 µm, 100 µm).

There is no bump compression for displacements inside the clearance region, thus the structural stiffness is only determined for the regions when $x > x_a$, and $x < x_b$. The bearing structural stiffness (K) for $x > x_a$ is,

$$K_{(z_1)} = \frac{\partial F}{\partial x} = K_{a1} + 3K_{a3}x^2 \qquad (3)$$

and for $x < x_b$

$$K_{(z_2)} = \frac{\partial F}{\partial x} = K_{b1} + 3K_{b3}x^2 \qquad (4)$$

Figure 8 shows the estimated bearing structural stiffness versus bearing deflection. The reduction in the bearing clearance associated to the shims aids to effectively increase the bearing structural stiffness. The stiffness hardening is nonlinear for both bearing orientations. The bearing structural stiffness for the 50 μm shimmed BFB configuration is 17% higher than the stiffness for the configuration without shims. At a load of 100 N the 100 μm shim bearing configuration has 45% higher stiffness than the configuration without shims. The estimated stiffness for a bearing with 100 μm shims shows a large structural stiffness (~2 MN/m) when the bearing has no deflection (not loaded) externally. This condition demonstrates that the bumps are being compressed prior to loading, thus evidencing a preload from an assembly interference.

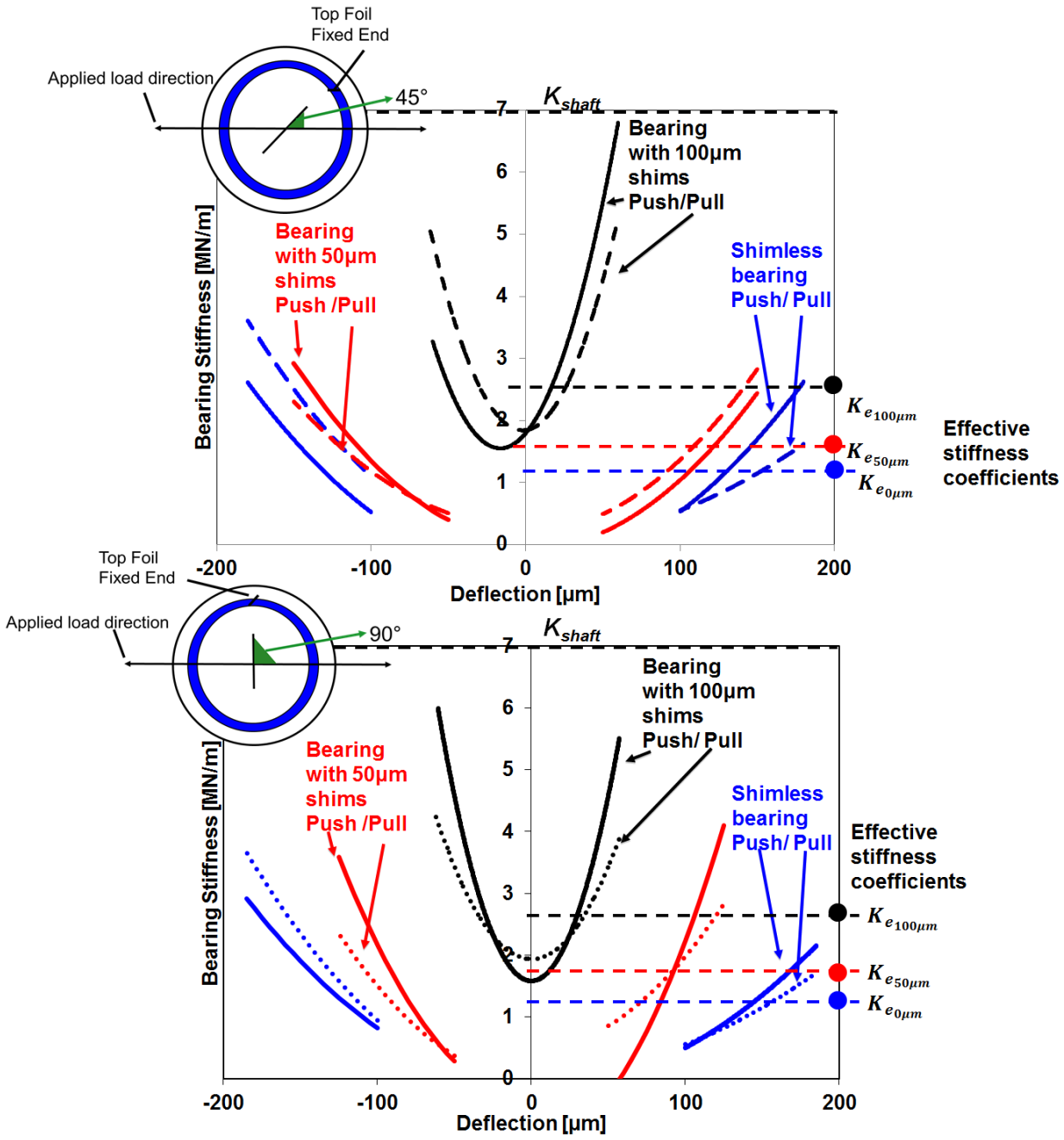

Fig. 8 Estimated FB structural stiffness versus FB deflection. 4 cycles of push and pull loads for (top) 45° (bottom) 90° bearing orientations. Results for three shim BFB configurations (0 μm, 50 μm, 100 μm).

Most of the identified bearing stiffnesses are lower than the stiffness of the shaft. The stiffness of the bearing with 100 μm shims approaches the stiffness of the shaft (K_s = 7 MN/m) at high loads (>150 N). Recall that the shaft deflection is subtracted from the measured displacements.

Results from the bearing deflection versus static load tests carried out on a BFB with and without shims show material hysteresis loops that evidence mechanical energy dissipation. The bearing material loss factor (γ) is a quantitative measure of the energy dissipation capability in a BFB. The estimation of the loss factor follows an analysis of the energy dissipation in the region of bump deflections shown in Figure 9.

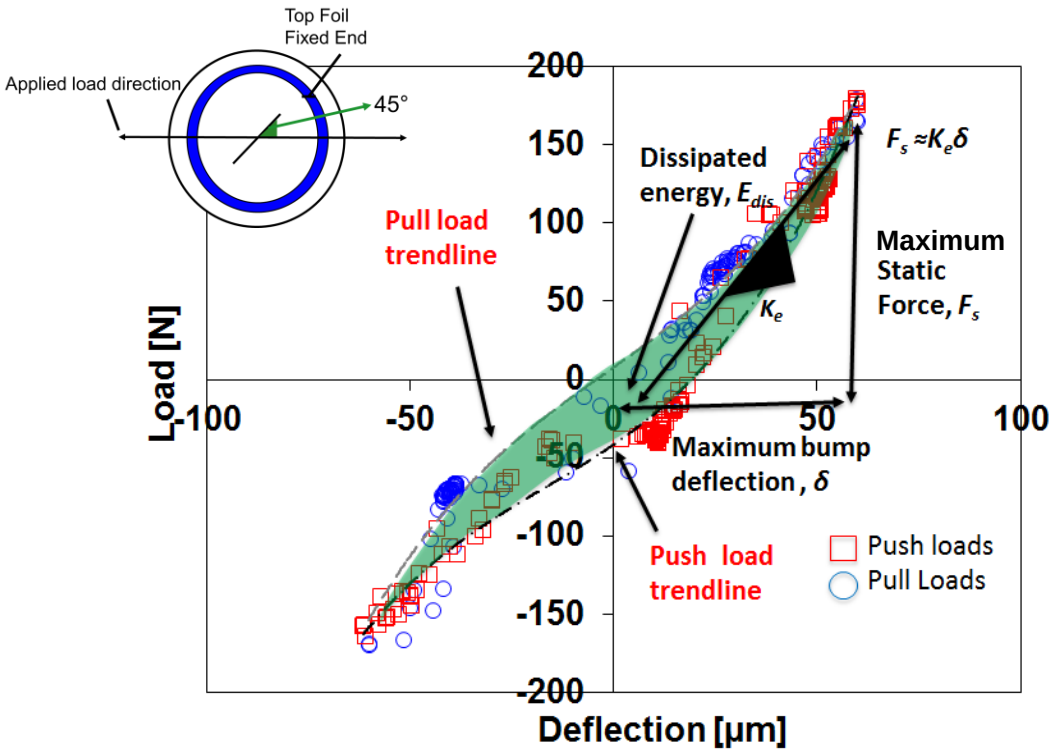

Fig. 9 Static load versus bearing deflection for a BFB with 100 μm, 45° orientation. Graph shows parameters for loss factor calculation.

The loss factor is defined in Ref. [8] as

$$\gamma = \frac{E_{dis}}{\pi K_e \delta^2} = \frac{\oint F_{(z)}\, dz}{\pi K_e \delta^2} \tag{5}$$

The mechanical energy dissipated (E_{dis}) is the area inside the material hysteresis loop. The curve fit equations extracted from the test results, presented in Table 4 and 5, are used to calculate E_{dis}. The load versus bearing deflection data presented in Figures 7 and 8 shows very little bump deflection for loads above 100 N. The maximum bump deflection (δ) at 100 N (F/LD=0.75 bar) is 60 μm, thus the maximum bump deflection for each shim BFB configuration is set to 60 μm. The maximum static load (F_s) and deflection (δ) estimated from the test results (refer to Figure 9b) are used to estimate an effective structural stiffness ($K_e \cong F_s/\delta$). Note that for

the BFB without shims and with 50 μm shims there is no energy dissipation over the diametral clearance as there is no bump compression; thus this region is excluded from the analysis.

Table 7 presents the estimated loss factors (γ) for each bearing configuration. The bearing dissipated mechanical energy (E_{dis}) and loss factor (γ) are sensitive to the bearing orientation. The 45° bearing orientation shows a larger dissipated energy and loss factors compared to the 90° bearing orientation. The magnitude of the effective stiffness (K_e) is consistent with the average structural stiffness estimated from $(\partial F/\partial x)$, and increases with increasing shim thicknesses.

Table 7 Estimated BFB dissipated energy (E_{dis}), effective stiffness (K_e), maximum bump deflection (δ), loss factor (γ).

Bearing Configuration		Dissipated Mechanical Energy, E_{dis} [Nm]	Effective Stiffness, K_e [MN/m]	Bump Maximum Static Displacement, δ [μm]	Loss Factor, γ
45°	Original	0.0010	1.22	60	0.07
	50 μm shims	0.0040	1.80	60	0.20
	100 μm shims	0.0016	2.66	60	0.07
90°	Original	0.0003	1.50	63	0.02
	50 μm shims	0.0027	1.80	60	0.13
	100μm shims	0.0012	2.66	60	0.05

The original bearing (without shims) has a very low loss factor ($\gamma \sim 0.02, 0.05$). Notice that the bearing with 50 μm shims show the highest loss factor ($\gamma \sim 0.13, 0.20$) while the bearing with 100 μm shims show a loss factor ($\gamma \sim 0.05, 0.07$) slightly above the loss factor of the original bearing.

The bearing with 50 μm shims dissipates a little more mechanical energy in the form of sliding friction between the bearing inner surface and the shaft. The bearing with 100 μm shims does not exhibit significant sliding friction between the bearing and the shaft due to its interference fit.

Prediction of BFB Structural Stiffness

The bump underspring layer creates a reaction force that opposes the force applied to the bearing. Rubio and San Andrés [7] produce a FB structural stiffness model based on Iordanoff's [9] single bump stiffness formulas. The model treats each bump as an individual spring element, uncoupled from its adjacent bumps thus it neglects the interaction of adjacent bumps and assumes the bump pitch remains constant. The predicted stiffnesses and loads are determined for the parameters listed in Table 1. The stiffness (per unit area) of a single bump with either both ends fixed (κ_w) and one end fixed and the other free (κ_f) are [9]

$$\kappa_w = \frac{E t_T^{\,3} \sin^3\left(\frac{\alpha}{2}\right)}{12\, l_o^3\, p\, J_{(\alpha)}(1-\nu^2)pL} \tag{6}$$

$$\kappa_f = \frac{E t_T^{\,3} \sin^3\left(\frac{\alpha}{2}\right)}{6\, l_o^3\, p\, I_{(\alpha)}(1-\nu^2)pL} \tag{7}$$

Above, E and ν are the elastic modulus and Poisson ratio respectively of the bump material: $J_{(\alpha)}$ and $I_{(\alpha)}$ geometric are functions of the bump arc (α). The bump pitch is denoted by p, the bump length half-length is l_o, and t_T is the top foil thickness. Also L is the bump strip axial length.

The simple predictive model evaluates the individual bump stiffness at their discrete locations around the bearing inner circumference. Structural stiffness predictions depend on the bump geometry and its end conditions (fixed or free), the direction of applied load, preload conditions, and a dry friction coefficient (μ_f). The model is modified to incorporate the effects of the three equally spaced shims. Load and structural stiffness versus FB deflection predictions are compared below against the experimental results. Note that the glue thickness is not taken into account.

Figure 10 and 11 presents the measured static load and structural stiffnesses versus the FB deflection and their model predictions for all bearing configurations with a 90° orientation. A dry friction coefficient, μ_f =0.15 is used for all predictions[1]. Predictions for a bearing without shims and with 50 μm shims are in good agreement with test data. Note that the predicted load versus bearing deflection curve for a bearing with 100 μm shims is wider than the experimental load versus deflection curve. The model predicts a larger clearance than the experimental results show. As a result the model underpredicts the structural stiffness coefficient at small bearing

[1] As reported in Ref. [8] for a bearing of the same materials in contact with a steel shaft

deflections (< 20 μm). For deflections larger than 20 μm the structural stiffness coefficient agrees well with the experimentally identified structural stiffness coefficient. Appendix A presents the predictions of static load versus BFB deflection as well as the bearing structural stiffness for the 45° BFB orientation.

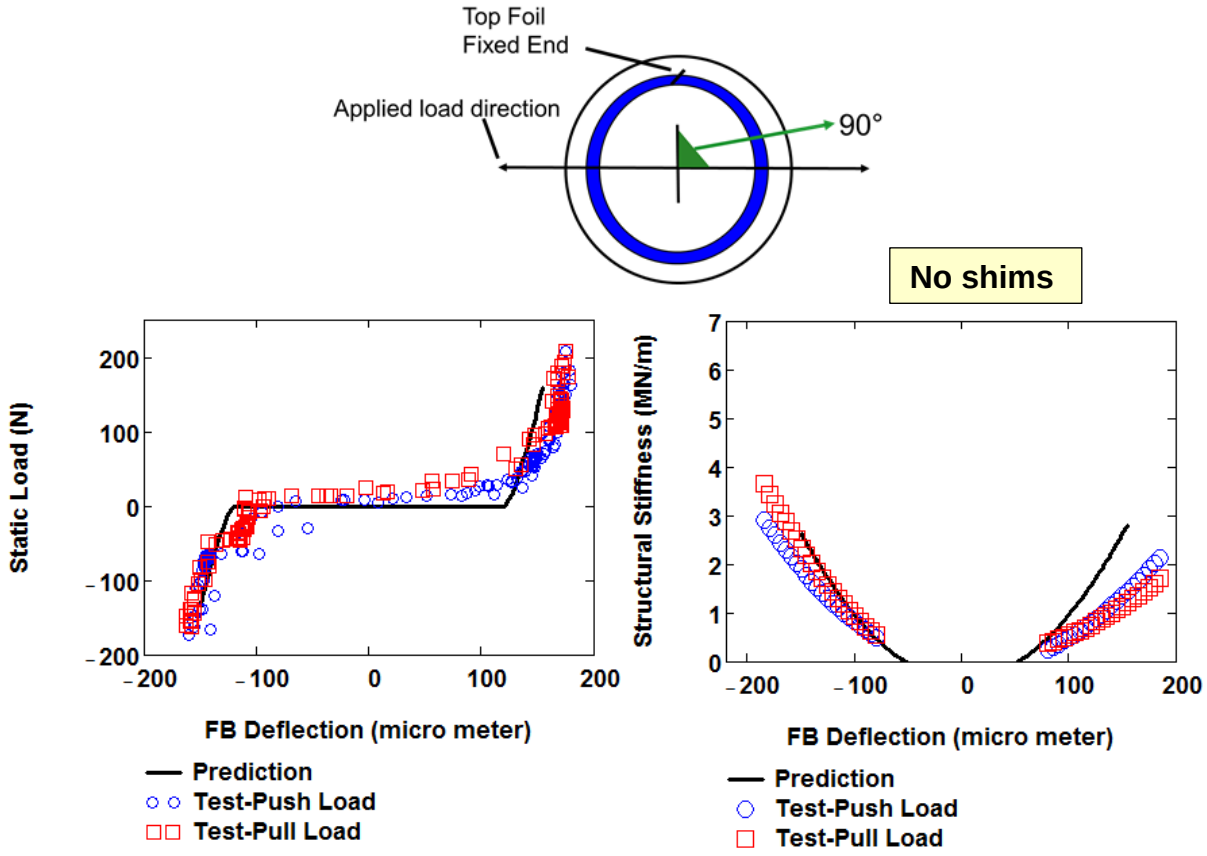

Fig. 10 Predicted and measured static load and bearing structural stiffness versus deflection for BFB without shims. 90° bearing orientation.

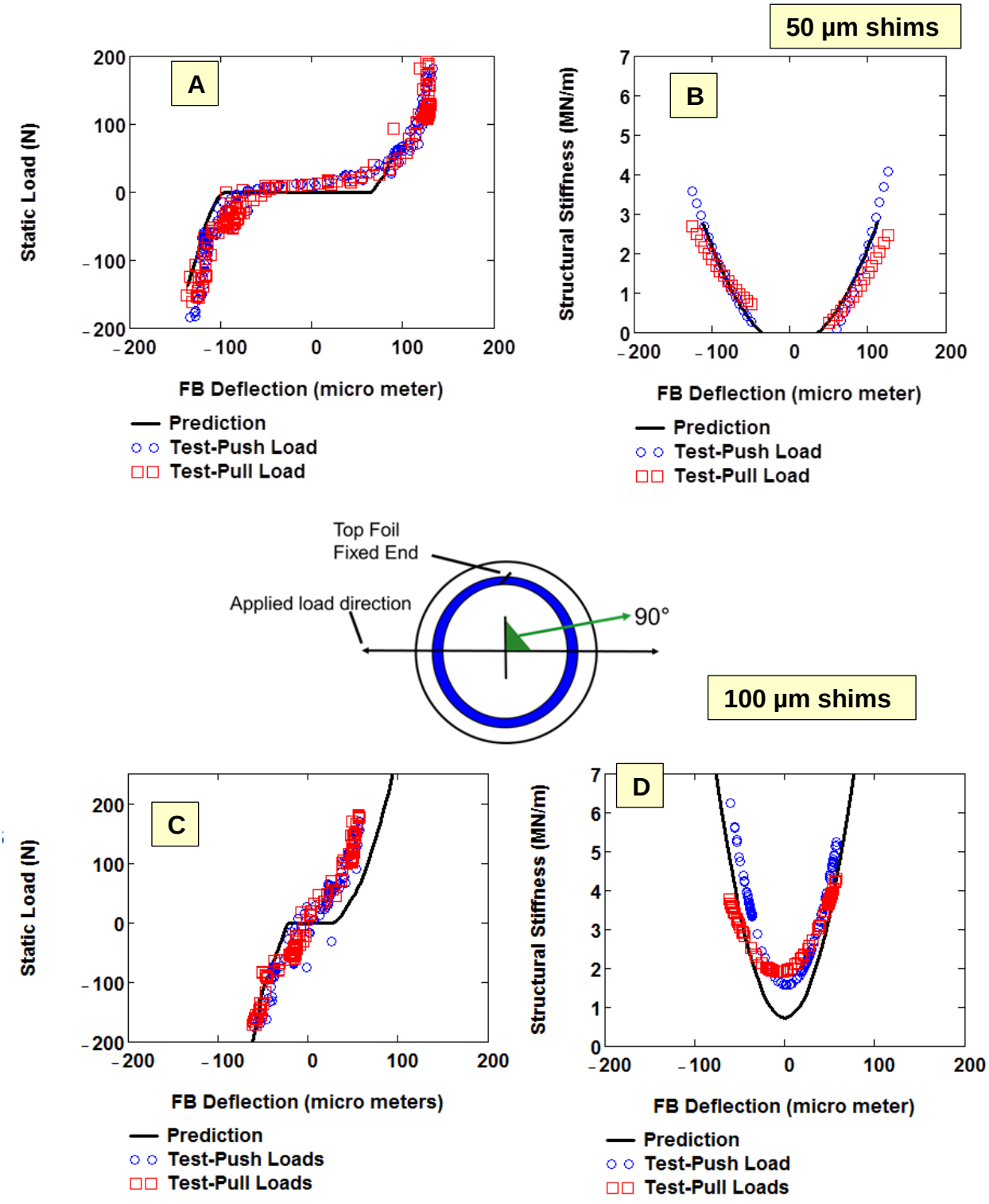

Fig. 11 Predicted and measured static load and bearing structural stiffness versus BFB deflection for (top) a bearing with 50 μm thick shims and for (bottom) a bearing with 100 μm thick shims. 90° bearing orientation.

Closure

This report presents the experimental estimation of structural stiffness coefficients (K) and structural loss factor (γ) for a bump type foil bearing with and without (3) shims for increasing static loads. Three steel shims (120°) of known nominal thickness are fitted under the bump foil strip of a test BFB creating a mechanical preload. Tests consist of recording the BFB deflection over a range of static loads of ± 200 N (F/LD=1.43bar).

The structural stiffness of the bearing is estimated from the load versus FB deflection test data. Test results show that shims effectively increase the bearing structural stiffness (up to 45% higher for a 100 N applied load). The increase in structural stiffness is non linear over the range of bearing deflections. The bearings load versus FB deflection behavior remains nonlinear for both bearing orientations and with the two shim thicknesses. Loading and unloading tests show miniscule hysteresis loops due to dry friction. The loss factor (γ) describes mechanical energy dissipation. The original bearing has quite a low loss factor $\gamma \sim 0.02\ (90°)$, and $0.05\ (45°)$. The bearing with 50 μm shims shows a significant increase in loss factor; $\gamma \sim 0.13\ (90°)$, and $0.20\ (45°)$. The bearing with 100 μm shims shows loss factors similar to the original bearing; $\gamma \sim 0.05\ (90°)$, and $0.07\ (45°)$. Predictions of stiffness based on a simple analytical formulation correlate well with the test results.

Dynamic load tests were performed with the same test bearing; however, the results are incongruent with the static load test results. Future work will seek to quantify the transient events (with a spinning rotor) of a shimmed BFB by identifying the startup and shut down drag torques, as well as the drag torque during airborne operation (journal rotation up to 50 krpm). It is also recommended to identify the rotordyanmic stiffness and damping coefficients of a shimmed BFB during airborne operation (with journal rotation). The results of the research will aid quantify the performance of shimmed gas foil bearings for improved rotordynamic performance.

References

[1] DellaCorte C., 2011, "Stiffness and Damping Coefficient Estimation of Compliant Surface Gas Bearings for Oil-Free Turbomachinery," STLE Tribol. Trans., **54** (4), pp. 674-684.

[2] Kim, T.H., and San Andrés., 2009, "Effects of a Mechanical Preload on the Dynamic Force Response of Gas Foil Bearings - Measurements and Model Predictions," STLE Tribol. Trans., **52**, pp. 569-580.

[3] Sim, K., Lee Y-B., Kim T.H., and Jangwon, L., 2012, "Rotordynamic Performance of Shimmed Gas Foil Bearings for Oil-Free Turbochargers," ASME J. Tribol., **134**, pp. 031102

[4] Kim, T.H., Rubio, D., and San Andrés, L., 2007, "Rotordynamic Performance of a Rotor Supported on Bump Type Foil Gas Bearings: Experiments and Predictions," ASME J. Eng. Gas Turbines Power, **129**, pp. 850-857.

[5] Kim, T.H., and San Andrés, L., 2008, "Forced Nonlinear Response of Gas Foil Bearing Supported Rotors," Trib. Int., **41**, pp. 704-715.

[6] Schiffmann, F., and Spakovszky, Z.S., 2013, "Foil Bearing Design Guidelines for Improved Stability," ASME J. Tribol., **135**, pp. 011103.

[7] Rubio, D., and San Andrés, L., 2006, "Bump-Type Foil Bearing Structural Stiffness: Experiments and Predictions," ASME J. Eng. Gas Turbines Power, **128**, pp. 653-660.

[8] Chirathadam, T.A., San Andrés, L., 2012, "A Metal Mesh Foil Bearing and a Bump-Type Foil Bearing: Comparison of Performance for Two Similar Size Gas Bearings," ASME J. Eng. Gas Turbines Power, **134**, pp. 102501.

[9] Iordanoff, I., 1999, "Analysis of an Aerodynamic Compliant Foil Thrust Bearing: Method for a Rapid Design," ASME J. Tribol., **121,** pp. 816–822.

Appendix A: Predictions of BFB Structural Stiffness (45° bearing orientation)

A simple formulation is used to calculate the static load (F) versus bearing deflection (x) behavior as well as to estimate the bearing structural stiffness coefficient. Predictions from this simple formulation are compared with experimental results for some of the bearing configurations. Results for the remaining bearing configurations are presented below.

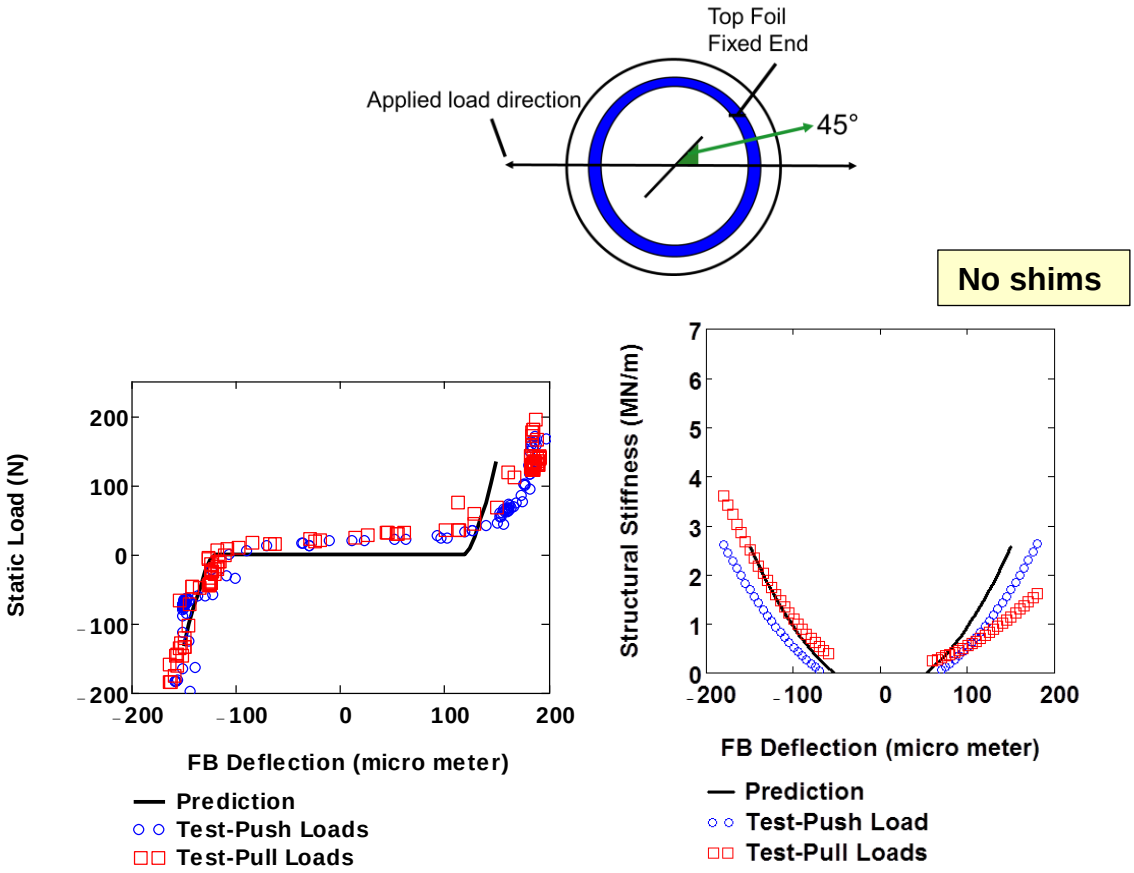

Fig. B1 Predicted and measured (left) static load and (right) bearing structural stiffness versus BFB deflection for a bearing with no shims 45° bearing orientation.

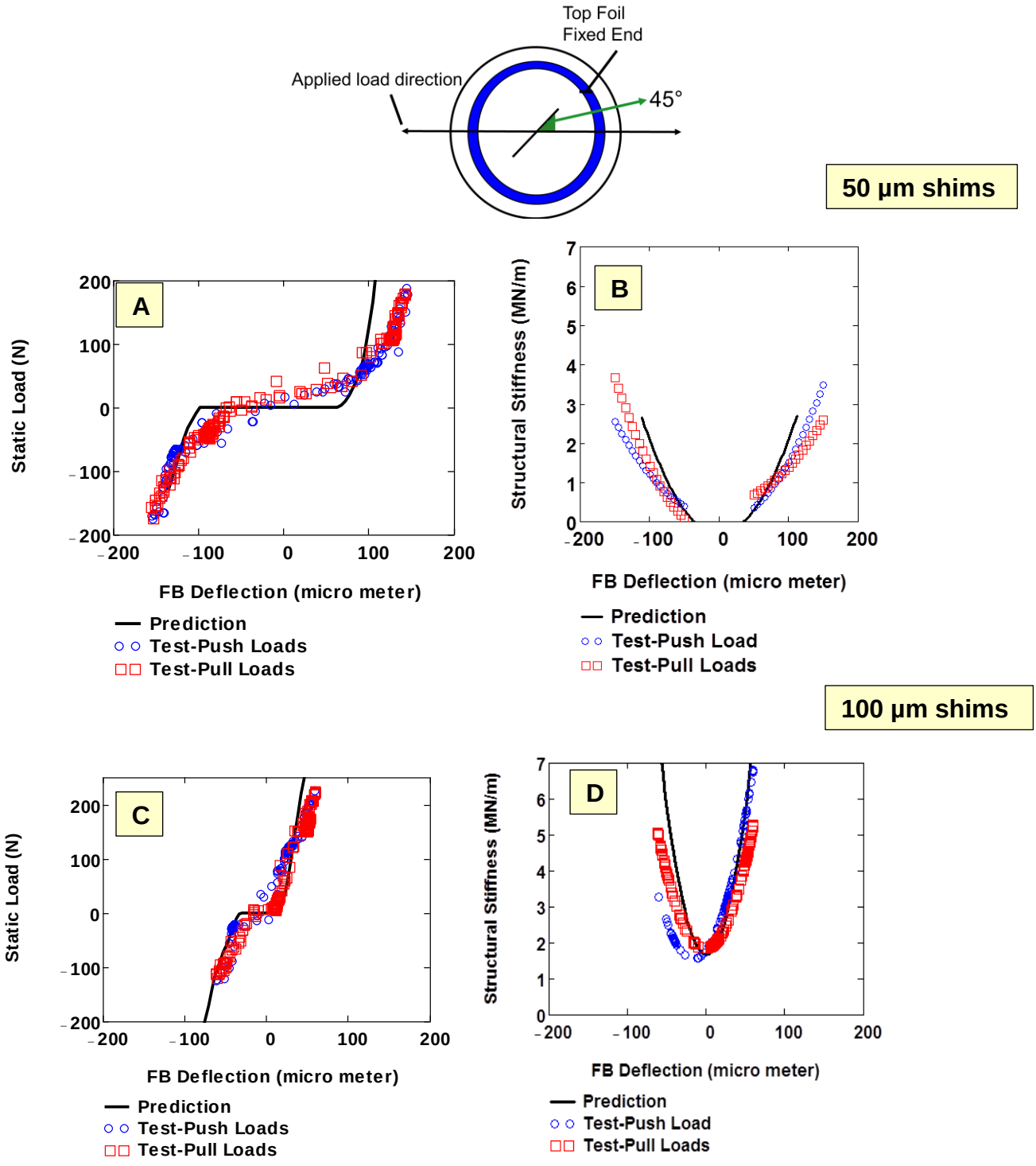

Fig. B2 Predicted and measured static load and bearing structural stiffness versus BFB deflection for (top) a bearing with 50 µm shims and for (bottom) a bearing with 100 µm thick shims. 45° bearing orientation.